Constructing Carbon-Coated Fe3O4 Hierarchical Microstructures with a Porous Structure and their Excellent Cr(VI) Ion Removal Properties

xiaoping wu
Zhejiang Sci-Tech University https://orcid.org/0000-0001-7163-5765
Lin Cheng
Zhejiang Sci-Tech University
Chang-Sheng Song
Zhejiang Sci-Tech University
Yi-Zhe Zhang
Zhejiang Sci-Tech University
Xiao-Jing Shi
Tongji Zhejiang College
Xiao-Yun Li
Zhejiang Sci-Tech University
Ping Lin
Zhejiang Sci-Tech University
Shun-Li Wang
Zhejiang Sci-Tech University
Peng Wang
Zhejiang Sci-Tech University
Ling-Bo Xu
Zhejiang Sci-Tech University
Li Jin
Zhejiang Sci-Tech University
Can Cui (cancui@zstu.edu.cn)
Zhejiang Sci-Tech University https://orcid.org/0000-0002-8429-5875

Research Article

Keywords: Fe3O4@C microstructures, magnetite, water treatment, heavy metals, adsorption

Posted Date: March 26th, 2021

DOI: https://doi.org/10.21203/rs.3.rs-335739/v1

Version of Record: A version of this preprint was published at Journal of Materials Science: Materials in Electronics on July 18th, 2021. See the published version at https://doi.org/10.1007/s10854-021-06600-3.

Abstract

Here, a facile solvothermal method coupled with an annealing strategy is developed to synthesize Fe_3O_4/carbon (Fe_3O_4@C) magnetic composite microstructures with different morphologies, including flower-like, hollow spheres and egg-like. Owing to the unique multi-porous and hollow structure, the as-prepared hierarchical Fe_3O_4@C hollow microspheres composite exhibit appealing performance as an absorbent of Cr(VI) ions in aqueous solution, delivering a high capacity of ca.197.2mg/g. Furthermore, the magnetic Fe_3O_4 “core” in composite hierarchical microstructures makes them easy to separate from aqueous systems by magnetic separation, the layer of carbon effectively prevents agglomerations of magnetic nanoparticles and expands their range of applications. The excellent Cr(VI) ions adsorbent activities of the Fe_3O_4@C magnetic composite microstructures would have a potential adsorbing material application in environmental purification.

1. Introduction

- Due to the toxicity of heavy metals and their non-degradability in the human body, water polluted with heavy metals has been a serious global environmental problem[1–4]. For example, Cr(VI) is a toxic heavy metal ion that can be easily absorbed by the human body and can enter the body through digestion, inhalation, skin and mucous membranes[5–8]. Cr(VI) has long-lasting environmental hazards, and has been identified as one of 17 highly most dangerous toxic substances. The oral lethal dose of Cr(VI) compounds is about 1.5 g. A Cr(VI) concentration above 0.1 mg/L in water will lead to poisoning of the drinking people. Long-term or short-term exposure or inhalation of Cr(VI) compounds may lead to cancer. A 0.1 mg/L Cr(VI) in irrigation water can inhibit the germination of rice seeds. The toxicity of Cr(VI) to the human body is similar to that of arsenic. The toxicity of Cr(VI) varies with valence, content, temperature and affected persons[9–13]. The emergence of more and more "cancer villages" is a warning that the removal of Cr(VI) has become urgent. Therefore, how to effectively remove Cr(VI) from water has become a key issue[14–18].

Many sewage treatment technologies, such as membrane filtration, biological oxidation, chemical precipitation, ion exchange, electrochemical and ion exchange methods, have been developed to remove pollutants in water[19–26]. However, these methods have some disadvantages such as a complicated operation process, high running cost and secondary pollution. Compared with other treatment technologies, adsorption separation technology has been widely used in waste water treatment because of its rich adsorbent resources, simple process and low cost. Therefore, the adsorption separation method is the most active research and application in recent years to remove toxic pollutants in sewage treatment methods[27–31]. It is well known that the adsorbent material is very important in the adsorption separation technology, but the existing adsorbent material still needs to be further improved, especially how to realize the fast separation and improve the adsorption performance of the material. With the development of magnetic materials and nanotechnology, the rapid separation and adsorption of materials can be realized in theory, so it brings new vitality to waste water treatment technology[32–36]. At

present, the development, research and application of magnetic nanomaterials have been paying great attention. Magnetic nanomaterials have many advantages, such as small particle size, large specific surface area, abundant surface active sites, strong magnetism, and so on. When used as an adsorbent, it can achieve high adsorption efficiency, quickly reach adsorption equilibrium, and under the effect of external magnetic field, it can be quickly separated from the liquid phase, avoiding common centrifugation or filtration treatment, and thus the difficulty and cost of the operation are greatly reduced. Therefore, magnetic nanomaterials have been widely used in the field of waste water treatment and attracted much attention[14,15,32–42].However, nanomaterials are easy to agglomerate because of their small size, which makes the preparation and application of nanomaterials difficult. Therefore, in recent years, magnetic adsorbents have been used to deal with water pollution problems, from the initial use of single magnetite as magnetic adsorbents to the synthesis of various surface modified functionalized magnetic nano-adsorbents to efficiently deal with pollutants in wastewater. Surface modification can not only improve the agglomeration of particles, but also modify the surface of nanomaterials according to the demand, so that the dispersibility, surface activity and compatibility with other materials can be improved, to make it more appropriate for the application[40–47]. In addition to introducing magnetism and surface modification, porous structure is also a widely used and effective method to improve the absorption capacity. The magnetic adsorbent is made into a porous structure, which increases the surface area, reduces the diffusion resistance, promotes the transfer of materials, and is beneficial to increase the adsorption capacity and speed up the adsorption[45–52]. Thus, at lower cost and facile synthetic method for the preparation of porous adsorbents with high specific surface area architectures for highly adsorption performance is still in great demand.

In this paper, we report a simple, template-free, and environmentally friendly route for the controlled synthesis of adjustable 3D Fe_3O_4@C micro-structures. The effect of the carbon source in the morphological control of Fe_3O_4@C micro-structures were discussed. Meanwhile, their removal performance in the adsorption of Cr(VI) ion was investigated in detail. The adsorbents can be quickly separated from their aqueous solution via an external magnet. The influence of the morphologies of Fe_3O_4@C composite micro-structures and the PH value of the solution for the adsorption performance were investigated. The results confirmed that Fe_3O_4@C hollow micro-spheres exhibited remarkable adsorption capacities for Cr(VI) ion with maximum uptake capacities of 197.2 mg/g.

2. Experimental Section

2.1 Materials.

Ferric chloride hexahydrate ($FeCl_3·6H_2O$)(A.R., Shanghai Chemical Co.), Triethylene tetramine (HETA) (A.R., Shanghai Chemical Co.), Hexamethylene tetramine (HMTA) (A.R., Shanghai Chemical Co.), Triethylene diamine (TEDA) (A.R., Shanghai Chemical Co.), Ethylene glycol (EG) (A.R., Hangzhou Chemical Co.), Hydrochloric acid (HCl) (A.R., Shanghai Chemical Co.), Sodium hydroxide (NaOH) (A.R.,

Shanghai Chemical Co.) and Potassium dichromate ($K_2Cr_2O_7$) (A.R., Guangzhou Chemical Co.). All of the reagents used in the experiment were directly used without further purification.

2.2 Synthesis of Fe_3O_4@C.

Growth of Fe_3O_4@C hollow spheres

In a typical experiment, first, 0.30 g (0.11 mmol) of $FeCl_3 \cdot 6H_2O$ were initially dissolved in EG (30 ml) and stirred vigorously at room temperature to give an orange solution. Next, 0.29 g (2 mmol) of Triethylene tetramine (HETA) was added into the orange solution. The resultant mixture was dispersed by continuously stirring the solution for about 30 min. After addition, the solution was transferred into a Teflon-lined stainless-steel autoclave with a volume of 40 ml, and subsequently sealed and heated at 160℃ for 6 h in an oven. After the heat treatment, the autoclave was cooled to room temperature naturally. The products were collected by centrifuging and washed several times with deionized water and absolute ethanol, and then dried at 60°C for 5h. The products were heated to 450°C at 7°C min^{-1} for 3h in N_2 in a horizontal furnace, leading to black Fe_3O_4@C powders.

Growth of Fe_3O_4@C flower-like and egg-shaped micro-structures: When the hexamethylene tetramine (HETA) and triethylene diamine (TEDA) were used to replace HETA, and other experimental conditions are consistent with the above, the morphologies of Fe_3O_4@C will form the flower-like and egg-shaped micro-structures respectively.

2.3 Characterization.

The morphology and the size of the as-prepared Fe_3O_4@C products were characterized using a Hitachi S-5500 Field-emission scanning electron microscope (FE-SEM, Tokyo, Japan), JEOL JEM-2010 high-resolution transmission electron microscope (HRTEM, Kyoto, Japan). Phase identification and structure analysis of the sample were carried out by Raman Spectroscopy (HORIBA, XploRA PLUS) and XRD using a Philips X' Pert Pro MPD X-ray diffractometer with Cu Ka radiation (λ = 0.154056 nm) operated at 40 kV and 40 mA in the 2θ range from 10–90° with a step size of 0.04° and a sampling time of 0.5s. The infrared (IR) spectrum was recorded using an AVATAR360 Fourier transform IR spectrophotometer at room temperature. Thermogravimetric and scalable differential thermal analysis (TG-SDTA) was carried out at a heating rate of 20°C min^{-1} in N_2 gas at a flowing rate of 50 ml min^{-1} using a PYRIS 1 TGA system. The specific surface areas of materials were performed by using surface area porosity analyzer (BSD-PS1).

2.4 Adsorption experiments.

$K_2Cr_2O_7$ was used as the source of Cr (VI). The different concentrations of Cr(VI) ions were prepared and the pH value was adjusted by HCl or NaOH. The fabricated different morphology of Fe_3O_4@C micro-structures were used as adsorbents for the removal of Cr(VI) ions from aqueous solutions. The adsorption experiments were performed on a digital water bath at 25°C. The adsorbent was then

separated from the mixture by a permanent magnet. To determine Cr (VI) ions removal by the adsorbent, the Cr(VI) concentration in the remaining solution was tested with a UV-vis spectrophotometer (UV-2600, Shimadzu). Ultraviolet light of 354 nm was used to irradiate the sample.

3. Results And Discussion

3.1. Characterization of Fe_3O_4@C hollow spheres. During the preparation of Fe_3O_4@C micro-structures, when HETA is used as carbon source, Fe_3O_4@C hollow spheres composed of thin slices can be formed. The morphology and size of the as-prepared Fe_3O_4@C hollow spheres are shown in Fig. 1(a-f). Figure 1a displays a representative overview of the Fe_3O_4@C hollow spheres, which shows that the prepared samples are composed of large-scale hollow spheres with diameters of 3μm. Figure 1b,c shows high-magnification SEM images of Fe_3O_4@C hollow spheres from a different angle of view, which vividly demonstrate that the Fe_3O_4@C hollow spheres are built of 2D nanoplates. From their TEM image in Fig. 1d-f, a clear, uniform shell of porous carbon layer was observed, indicating the successful coated of the carbon layer in the Fe_3O_4 and the formation of Fe_3O_4@C nanoplates. The nanoplates are well-ordered and oriented to form Fe_3O_4@C hollow spheres. The XRD pattern of the typical sample prepared at 160°C for 6 h is shown in Fig. 2a. The diffraction peaks of as-synthesized sample can be indexed to the cubic Fe_3O_4 with lattice constants of a = b = c = 8.397 Å, which agrees with the standard XRD databases (JCPDS, Card No. 79–0419; space group: Fd-3m(227)). The major XRD diffraction peaks appeared at 2θ = 29.93, 35.32, 42.91, 56.90, and 62.43°, attributed to (220), (311), (400), (511), and (440) planes, can be seen clearly. No obvious peaks resulting from impurities were observed, indicating a high purity Fe_3O_4 sample. As shown in Fig. 2b, the elemental analysis performed by EDS demonstrates that our samples are mainly contained Fe, O and C elements. Further, according to the area of the peaks the ratio of Fe to O in single hollow spheres micro-structure is about 3:5, of which O was slightly excessive, mainly from the conductive adhesive of the substrate material. Which can demonstrate that a 3:4 Fe/O composition within experimental error is consistent with stoichiometric (3:4) Fe_3O_4. At the same time, the results showed that the synthetic product contained about 10 Wt% carbon. Combined with the high-magnification SEM and TEM images, we believed that there was a layer of carbon on the surface of Fe_3O_4 sheet, so the hollow sphere should be Fe_3O_4@C hollow spheres, which we will further prove by Raman test later.

The compositions of Fe_3O_4@C hollow spheres were further confirmed by Fourier transform infrared spectroscopy are shown in Fig. 3. For comparison, unannealed sample (Fe_3O_4@$(HMTA)_n$) (Fig. 3a) and Fe_3O_4@C hollow spheres (Fig. 3b) were measured by FTIR. For example, the absorption peaks at 2839cm^{-1}can be assigned to the C-H symmetrical stretching vibrations, the absorption band at 1080 cm^{-1} is attributed to the C-N stretching vibrations, and the two sharp peaks at 891 and 828 cm^{-1} are assigned to the C-H out-of-plane deformation vibrations. Peaks around 1360 cm^{-1} are referred to C = O stretching band or C = C stretching vibration. The characteristic peak of Fe_3O_4@C at 561 cm^{-1} (Fe-O stretching of Fe_3O_4) in curve 3b was also detected in Fe_3O_4@$(HETA)_n$ an inside curve 3a marked by a

rectangle frame. The relatively low intensity of the band at 551 cm^{-1} in Fe_3O_4@$(HETA)_n$ indicates the low content of Fe_3O_4 in the Fe_3O_4@(organics) composite micro-structures, this was further proved by the following TG analysis. The results of the TG-DTA analysis of the Fe_3O_4@$(HETA)_n$ composite micro-structures are shown in Fig. 4. The initial mass loss is observed from room temperature to 300°C mainly due to the release of water from the Fe_3O_4@$(HETA)_n$ composite micro-structures. The endothermic peak at 335°C corresponds to the decomposition of Fe_3O_4@HETA composite micro-structures. From the TG analysis, the mass ratio of the Fe_3O_4 in the Fe_3O_4@$(HETA)_n$ composite is about 41.9 wt%. Which is close to the expected value of 43.2% calculated from the change of Fe_3O_4@$(HETA)_{1.5}$ to Fe_3O_4@$(C)_2$, which is consistent with the EDS data. These results reveal that the unannealed samples are a type of Fe_3O_4@$(HETA)_n$ hybrid compound, Fe_3O_4@$(HETA)_{1.5}$.

3.2. Influence of carbon source on the morphology evolution of hierarchical Fe_3O_4@C micro-structures.

In the research process, we found that carbon sources had a great influence on the morphology of hierarchical Fe_3O_4@C micro-structures. To identify the role of carbon source in the formation of Fe_3O_4@C micro-structures, the products obtained under the circumstance of different carbon source (HMTA, HETA, TEDA) were characterized by SEM and TEM, as shown in Fig. 5. Figure 5a-c shows the SEM and TEM images of the product obtained in the solvothermal system with the carbon source is HMTA. It can be seen that the products is composed of hierarchical flower-like micro-structures with the diameters of about 4.5μm. When the carbon source is changed to HETA, the self-assembled architecture became apparently hollow spheres with an average diameter of 3μm as shown in Fig. 5d-f. As shown in Fig. 5g-i, as the carbon source converts to TEDA, the products are uniform egg-like Fe_3O_4@C composite micro-spheres composed of flakes with sizes of about 3.5μm. In addition, the products with three different morphologies were characterized by XRD and the results showed that the products with three different morphologies were Fe_3O_4 as shown in Fig. 6.

In order to prove the existence of carbon layer on the surface of Fe_3O_4, it is further confirmed by the Raman spectroscopy analysis in the range from 500 to 2000 cm^{-1} as shown in Fig. 7. Which showed that a D band at 1324-1361cm^{-1} and a G band at 1573-1587cm^{-1} herein originate from finite-size crystals of graphite and amorphous C sp2 sites, respectively, and the band around 688cm^{-1} was observed, which correspond to the Fe-O bond for spinel Fe_3O_4 particles. This result is in agreement with the XRD result, confirming that the samples of three different morphologies composite are composed of the magnetite Fe_3O_4 phase and amorphous carbon. Therefore, the results indicate that the carbon source played an important role in the formation and the assembly of hierarchical Fe_3O_4@C micro-structures. Of course, we're not looking at why carbon sources affect the morphology of Fe_3O_4. Our next job is to understand how and why the Fe_3O_4 samples grow into such multiform structures.

3.3 Study on Cr(VI) ion adsorption properties of three different morphologies Fe_3O_4@C micro-structures.

We have carried out heavy metal ion adsorption test on the Fe_3O_4@C hollow spheres, the PH value of the solution is an important parameter in the adsorption of heavy metals, which can not only change the

existing form of heavy metal ions, but also change the charge of the functional group on the surface of the adsorbent. Therefore, it is necessary to investigate the effect of the PH value of the solution to the adsorption performance. To get a full understanding about the effect of PH value on the adsorption property of materials, we performed a number of experiments with various PH values(1, 2, 3, 4, 7, 12, 13) are shown in Fig. 8. It can be seen that the reduction efficiency of Cr(VI) increases by increasing the acidity of the solution and the maximal removal was at PH value is equal to 2. However, when the PH value is alkaline, there is almost no adsorption of Cr(VI) ions. We think that there are two reasons for the good adsorption performance under acidic conditions. First, under acidic conditions, Fe_3O_4 is easy to hydrolyze into $Fe(OH)_2^+$, which has a reduced effect of Cr(VI) ions. The highly toxic hexavalent Cr(VI) ions can be reduced to the less toxic trivalent Cr(III) ions. Secondly, under acidic conditions, Cr(VI) ions are mainly in the form of negatively charged $Cr_2O_7^{2-}$ and $HCrO_4^-$. When Cr(VI) ions contact with the material, the Cr(VI) ions are absorbed to the surface of the material under the joint action of surface adsorption and electrostatic attraction.

In waste water treatment, the adsorption efficiency of adsorption materials is an important parameter. Therefore, we investigated the adsorption performance of Fe_3O_4@C composite micro-structures with different morphologies at room temperature when the PH value is equal to 2 (Fig. 9). For instance, when 50 mg of as-prepared Fe_3O_4@C composite micro-structures were dispersed into a 100 ml solution of $K_2Cr_2O_7$ at a concentration of 100 mgL^{-1}, more than 80% of the Cr(VI) in the solution could be absorbed within 30 min, as illustrated in Fig. 8. The magnetic separability, dispersibility and water solubility of the obtained Fe_3O_4@C composite micro-structures were tested in the adsorption process by placing an external magnetic field near the glass bottle as shown by the digital photograph in the inset of Fig. 9a-c. The original color of the $K_2Cr_2O_7$ solution with a concentration of 100 mg L^{-1} was buff (inset Fig. 9a), with a slight agitation, the obtained Fe_3O_4@C composite micro-structures disperses into the $K_2Cr_2O_7$ aqueous solution, the color of the solution changes to black (inset Fig. 9b). These magnetic composite micro-structures can be completely separated from the solution when the solution is subjected to an external magnetic field within minutes, as shown inset Fig. 9c. The obvious change of color from buff to colorless indicated that the obtained composite micro-structures possessed excellent adsorption and magnetic properties. In addition, the good dispersion of the Fe_3O_4@C composite micro-structures in $K_2Cr_2O_7$ solution are conducive to the adsorption of Cr(VI) ions (inset Fig. 9b). By comparative analysis of Cr(VI) in the supernatant obtained by centrifugation and after magnetic separation, it is found that there is basically no difference, indicating that the Fe_3O_4@C composite micro-structures can be used to remove Cr(VI) from aqueous solutions and recovered by using a magnetic separation technique in practical application. The above results show that the adsorption performance of the Fe_3O_4@C hollow spheres is the best. However, the specific surface area, pore size and special material surface functional groups in the adsorption performance of materials plays an important role, therefore, to study what factors influence the adsorption properties of Fe_3O_4@C composite micro-structures, we have three different morphology of Fe_3O_4@C composite micro-structures for the study of N_2 adsorption-desorption measurements and infrared spectrum (Fig. 10,11).

The porous structures of flower-like, hollow spheres and egg-like Fe_3O_4@C composite micro-structures are incurred by N_2 adsorption-desorption measurements and the results are shown in Fig. 10. Interestingly, the specific surface area of flower-like Fe_3O_4@C composite micro-structures is the largest, but its adsorption property is the worst, we think the flower-like Fe_3O_4@C porous pore between main carbon particles(the pore size is concentrated at 3.6nm), Cr(VI) don't have much chance of coming into contact with the Fe_3O_4 and result in low adsorption performance. The specific surface area of the egg-like Fe_3O_4@C is only about half of that of the other two structural materials. We believe that the "egg yolk" is solid, leading to a sharp decrease in the specific surface area, thus resulting in poor adsorption performance of Cr(VI) ions. The pore size of hollow spheres Fe_3O_4@C is mainly concentrated at 12 nm. We believe that the pore size of hollow spheres Fe_3O_4@C is mainly between carbon particles and Fe_3O_4, that chromium ions can fully contact with Fe_3O_4, so that its adsorption performance is relatively good.

In order to exclude the influence of functional groups on the surface of the material on adsorption performance, infrared tests were conducted on the samples of three different morphologies for comparison, as shown in Fig. 11. The results show that the surfaces of the three structures are consistent after annealing, and there is no special functional group on the surface, so the effects of surface functional groups on adsorption properties are excluded. In conclusion, it is believed that the specific surface area and pore size of the material are the important factors affecting the adsorption performance of heavy metals in Fe_3O_4@C composite micro-structures.

4. Conclusion

In summary, we demonstrate a novel and facile synthetic route for the synthesis of multi-morphology Fe_3O_4@C magnetic composite micro-structures, including flower-like, hollow spheres, and egg-like. This simple method does not need the subsequent complicated workup procedure required for the removal of the template or seed. On the basis of synthesis reactions, carbon source acted as an important parameter for the synthesis, reactions and the shape controller for the crystal growth of flower-like, hollow spheres, and egg-like micro-structures. The results indicate that this method may also be further extended to control the growth of versatile Fe_3O_4@C crystals, which may find application in many fields. Simultaneously, these Fe_3O_4@C magnetic composite hollow micro-spheres were shown to be an excellent Cr(VI) ions adsorbent, which allows them to serve as ideal candidates for environmental remediation materials.

Declarations

Author contributions

The manuscript was written through contributions of all authors. All authors have given approval to the final version of the manuscript.

Acknowledgment

This research was supported by the Zhejiang Provincial Natural Science Foundation of China (Grant No. LQ18E020003 and LY20F040005), Open Foundation of Key Laboratory of Optical Field Manipulation of Zhejiang Province (ZJOFM-2020-006), Basic scientific research operating expenses of Zhejiang University of Science and Technology (2019Q073), National Natural Science Foundation of China (Grant No. 51672249).

References

[1] M. Hua, S. J. Zhang, B. C. Pan, W. M. Zhang, L. Lv, Q. X. Zhang, *J. Hazard. Mater.,* 211-212, 317(2012).

[2] A. Latif, D. Sheng, K. Sun, Y. B. Si, M. Azeem, A. Abbas, M. Bilal, *Environ. Pollut.,* 264, 114728(2020), .

[3] Q. Wang, Z. M. Yang, *Environ. Pollut.,* 218, 358(2016).

[4] S.Bolisetty, M. Peydayesh, R. Mezzenga, *Chem. Soc. Rev.,* 48, 463(2019).

[5] B. Novotnik, J. Ščančar, R. Milačič, M. Filipic, B. Zegura, *Chemosphere,* 154, 124(2016).

[6] J. H. Park, *Environ. Pollut.,* 266, 115073(2020).

[7] Q. Zhang, Y. Z. Song, K.Amor, W.E. Huang, D. Porcelli, I. Thompson, *Water Research,* 153, 295(2019).

[8] L. Qin, G. Zeng, C. Lai, D. L. Huang, P. A. Xu, C. Zhang, M. Cheng, X. G. Liu, S. Y. Liu, *Coord. Chem. Rev.,* 359, 1(2018).

[9] W. Jin, H. Du, S. Zheng, Y. Zhang, *Electrochim. Acta,* 191, 1044(2016).

[10] A. M. Latifi, M. Mirzaei, M. M. Kamazani, Z. Zarghami, *J. Mater.Sci.:Mater.Electron.,* 29, 10234(2018).

[11] S.H.Chen, J. Zhang, C. L. Zhang, Q.Y. Yue, Y. Li, C. Li, *Desalination,* 252, 149(2010).

[12] X. Chen, Y. Hou, B. Zhang, X. H. Yang, H. G. Yang, *Chem. Commun.,* 49, 5793(2013).

[13] M. Basu, A. K. Sinha, M. Pradhan, S. Sarkar, Y. Negishi, Govind, T. Pal, *Environ. Sci. Technol.* 44, 6313(2010).

[14] Y. Q. Wang, B.F. Zou, T. Gao, X. P. Wu, S. Y. Lou, S. M. Zhou, *J. Mater. Chem.,* 22, 9034(2012).

[15] Y. B. Liu, Y. Q. Wang, S. M. Zhou, S. Y. Lou, L. Yuan, T. Gao, X. P. Wu, X. J. Shi, K. Wang, *ACS Appl. Mater. Interfaces,* 4, 4913(2012).

[16] W. C. Cheng, C. C. Ding, X. X. Wang, Z. Y. Wu, Y. B. Sun, S. H. Yu, T. Hayat, X. K. Wang, *Chem. Eng. J.,* 293, 311(2016).

[17] D. Dinda, A. Gupta, S. K. Saha, *J. Mater. Chem. A.,* 1,11221(2013).

[18] J. Li, L. X. Xie, R. Guo, H. Wang, Z. P. Liang, H. Q. Yao, S. L. Ma, *J. Alloy. Compd.,* 823, 153519(2020).

[19] S. Y. Hong, R. Popovitz-Biro, Y. Prior, R. Tenne, *J. Am. Chem. Soc.,* 125, 10470(2003).

[20] A. Ullah, S. Hussain, A. Wasim, M. Jahanzaib, *Sci.Total Environ.,* 731, 139158(2020).

[21] S. D. Melvin, F. D. L. Leusch, *Environ. Internat.,* 92-93, 183(2016).

[22] H. Yi, G. M. Zeng, C. Lai, D. L. Huang, L. Tang, J. L. Gong, M. Chen, P. Xu, H. Wang, M. Cheng, C. Zhang, W. P. Xiong, *Chem. Eng. J.,* 330, 134(2017).

[23] Y. H. Wu, H.W. Pang, Y. Liu, X. X. Wang, S. J. Yu, D. Fu, J. R. Chen, X. K. Wang, *Environ. Pollut.,* 246, 608(2019).

[24] H. C. Vu, A. D. Dwivedi, T. T. Le, S. H. Seo, E. J. Kim, Y. S. Chang, *Chem. Eng. J.,* 307, 220(2017).

[25] S. Rengaraj, C. K. Joo, Y. Kim, J. H. Yi, *J. Hazard. Mater.,* 102, 257(2003).

[26] G. D. Sheng, J. Hu, H. Li, J. X. Li, Y. Y. Huang, *Chemosphere,* 148, 227(2016).

[27] C. Gutierrez, H. K. Hansen, P. Nunez, E. Valdes, *Electrochim. Acta,* 181, 228(2015).

[28] S. Sessarego, S. C. G. Rodrigues, Y. Xiao, Q. Y. Lu, J. M. Hill, *Carbohydrate Polymers,* 211, 249(2019).

[29] X. W. Li, Q. Q. Mei, L. B. Chen, H. Y. Zhang, B. Dong, X. H. Dai, C. Q. He, J. Zhou, *Water Research,* 157, 228(2019).

[30] Z. F. Yin, C. J. Cui, H.Chen, Duoni, X. Yu, W. Z. Qian, *Small,* 16, 1902301(2020).

[31] P. M. Alvárez, F. J. Beltrán, F. J. Masa, J. P. Pocostales, *Appl. Catal. B: Environ.,* 92, 393(2009).

[32] Y. J. Yang, L. J. Xu, W. Y. Li, W. J. Fan, S. Song, J. Yang, *Appl. Catal. B: Environ.,* 259, 118057(2019).

[33] S. Maryam, H. Maryam, J. Vahid, *J. Mater.Sci.: Mater. Electron.* 32, 5065(2021).

[34] H.S. Far, M. Hasanzadeh, M. S. Nashtaei, M. Rabbani, A. Haji, B. H. Moghadam, *ACS Appl. Mater. Inter.,* 12, 25294(2020).

[35] X. X. Yao, L. L. Ji, J. Guo, S. L. Ge, W. C. Lu, L. Cai, Y. N. Wang, W. D. Song, H. L. Zhang, *Bioresource Technol.,***302**, 122842(2020).

[36] X. Y. Zheng, H. L. Zheng, Z. K. Xiong, R. Zhao, Y. Z. Liu, C. Zhao, C. F. Zheng, *Chem. Eng. J.,***392**, 123706(2020).

[37] M. Hassan, R. Naidu, J. H. Du, Y. J. Liu, F. J. Qi, *Sci. Total Environ.,* 702, 134893(2020).

[38] M. Mitra, H. Y. Aziz, P. Shima Rahim, *J. Mater. Sci.: Mater. Electron.* 29, 1719(2018).

[39] X. D. Liu, J. F. Tian, Y. Y. Li, N. F. Sun,S. Mi,Y. Xie,Z. Y. Chen,*J. Hazard. Mater.,* 373, 397(2019).

[40] L. Guo, Q. D. An, Z. Y. Xiao, S. R. Zhai, L. Cui, *ACS Sustain. Chem. Eng.,* 7, 9237(2019).

[41] Y. H. Wang, C. Y. Lin, Z. W. Wang, Z. M. Chen, J. F. Chen, Y. Chen, S. H. Liu, J. W. Fu, *J. Colloid. Interf. Sci.,* 556, 278(2019).

[42] X. Zhong, Z. P. Lu, W. Liang, B. W. Hu, *J. Hazard. Mater.,* 393, 122353(2020).

[43] L. Zhou, M. Z. Xu, G. D. Wei, L. Li, M. V. Chubik, M. P. Chubik, A. A. Gromov, W. Han, *J. Mater. Sci.: Mater. Electron.,* 26, 2742(2015).

[44] Q. U. Ain, H. B. Zhang, M. Yaseen, U. Rasheed, K. Liu, S. Subhan, Z. F. Tong, *J.Clean. Prod.,* 247, 119088(2020).

[45] Y. Fang, J.Wen, H.B. Zhang, Q. Wang, X. H. Hu, *Environ. Pollut.,* 260, 114021(2020).

[46] N.T. Abdel-Ghani, G. A El-Chaghaby, E. S. A. Rawash, E. C. Lima, *J. Adv. Res.,* 17, 55(2019).

[47] G. F. Liu, L. Liao, Z. M. Dai, Q. Qi, J. Z. Wu, L. Q. Ma, C. X. Tang, J. M. Xu, *Chem. Eng. J.,* 395, 125108(2020).

[48] Y. Z. Shi, S. X. Deng, B. H. Zhao, B. H. Zhao, Y. J. Fu, Z. G. Liu, *Chem. Phys. Lett.,* 753, 137600(2020).

[49] T. Wang, L. W. Zheng, Y. H. Liu, W. Tang, T. Fang, B. S. Xing, *Sci. Total Environ.,* 730, 138928(2020).

[50] E. A. Dil, A. Asfaram, F. Sadeghfar, *Analyst,* 144, 2684(2019).

[51] E. Yavuz, S. Tokalioglu, S. Patat, *Food Chem.,* 263, 232(2018).

[52] B. Y. Huang, Y. G. Liu, B. Li, S. B. Liu, G. M. Zeng, Z. W. Zeng, X. H. Wang, Q. M. Ning, B. H. Zheng, C. P. Yang, *Carbohyd. Poly.,* 157, 576(2017).

Figures

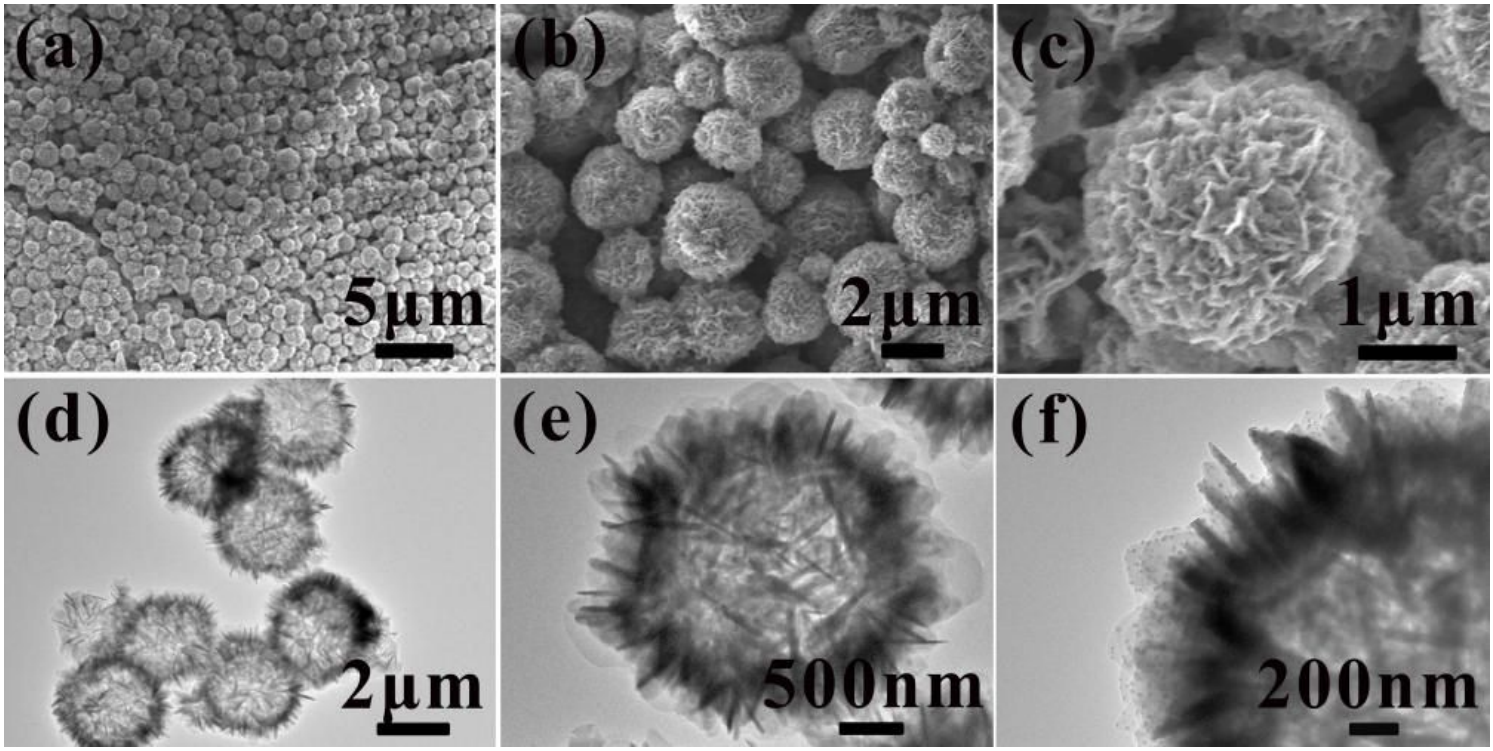

Figure 1

(a) Low magnification SEM, (b,c) high magnification SEM and (d-f) TEM of Fe3O4@C hollow spheres microstructures.

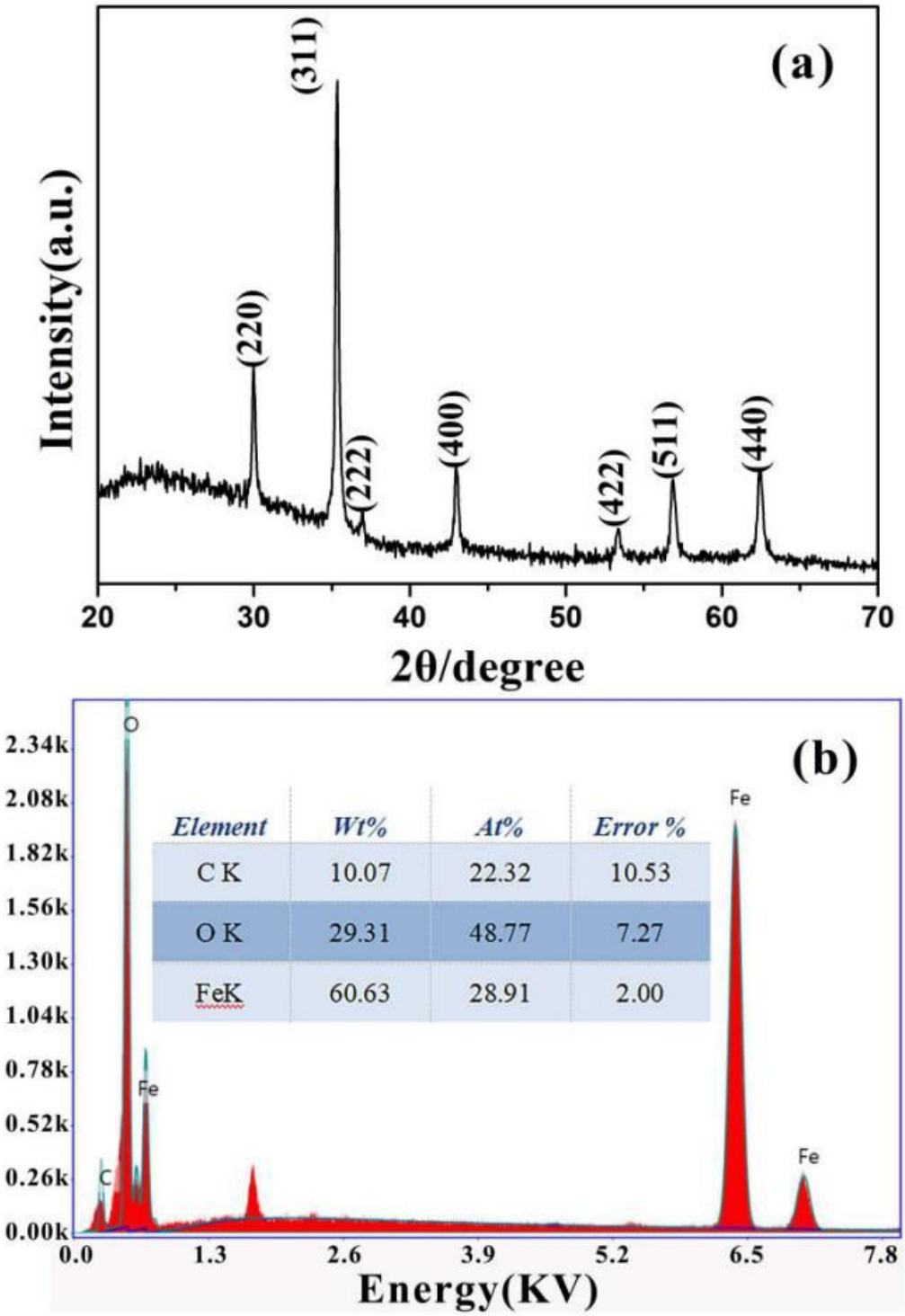

Figure 2

(a) XRD patterns and (b) EDS spectra of Fe3O4@C hollow spheres.

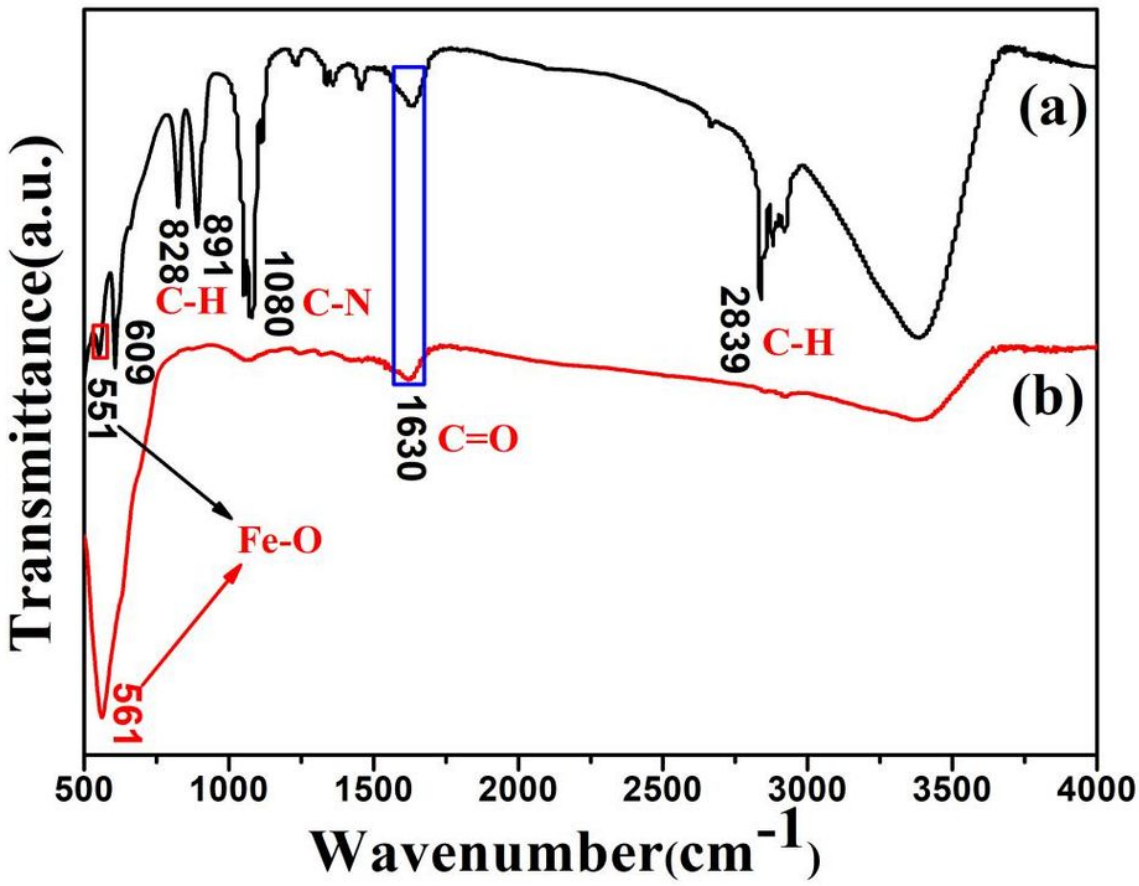

Figure 3

FTIR spectra of (a) Fe3O4@HMTA hollow spheres (before annealing), (b) Fe3O4@C hollow spheres (after annealing).

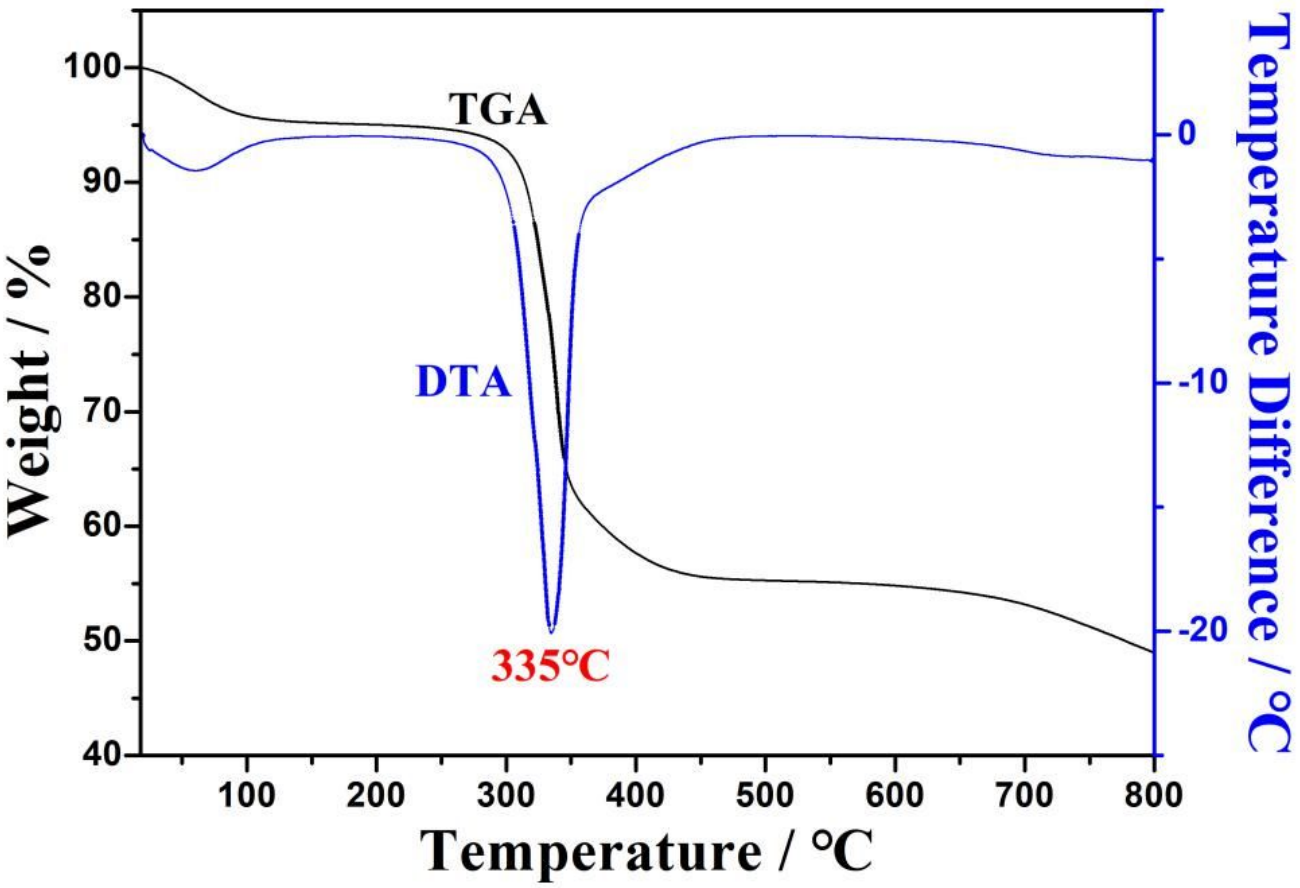

Figure 4

TG-DTA curves of Fe3O4@HMTA hollow spheres (before annealing).

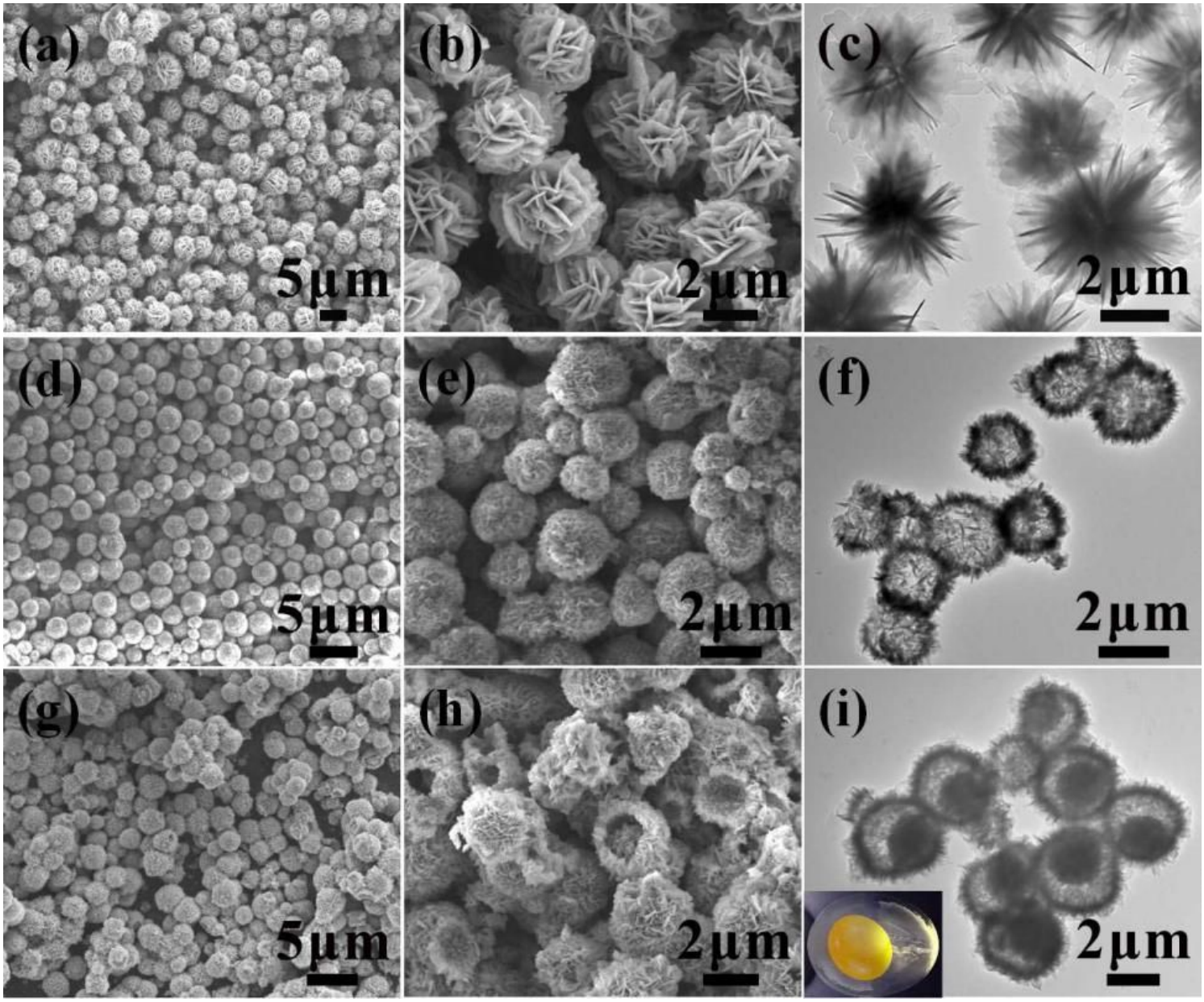

Figure 5

SEM images of Fe3O4@C microstructures obtained at different carbon source: (a,b) HMTA, (d,e) HETA, (g,h) TEDA. TEM images of Fe3O4@C microstructures obtained at different carbon source: (c) HMTA, (f) HETA, (i) TEDA.

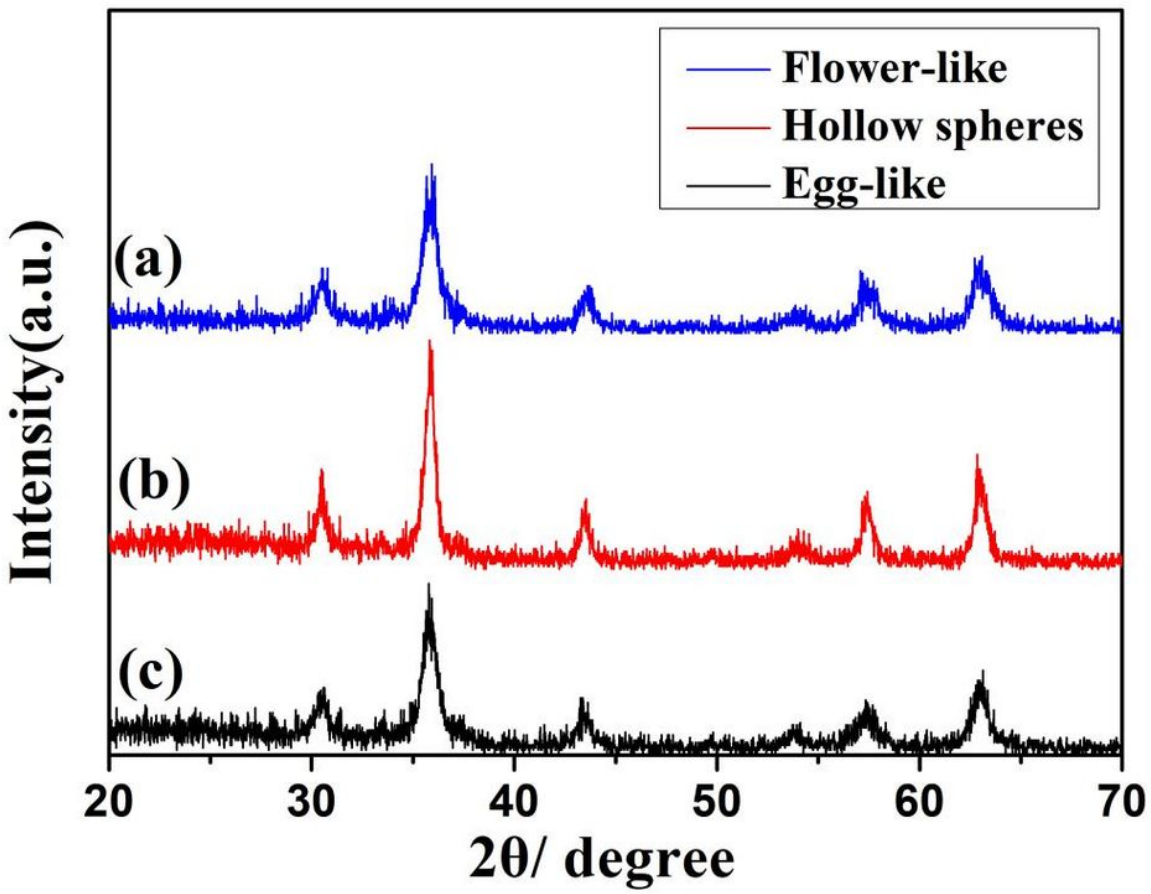

Figure 6

XRD patterns of Fe3O4@C flower-like, hollow spheres, and egg-like microstructures.

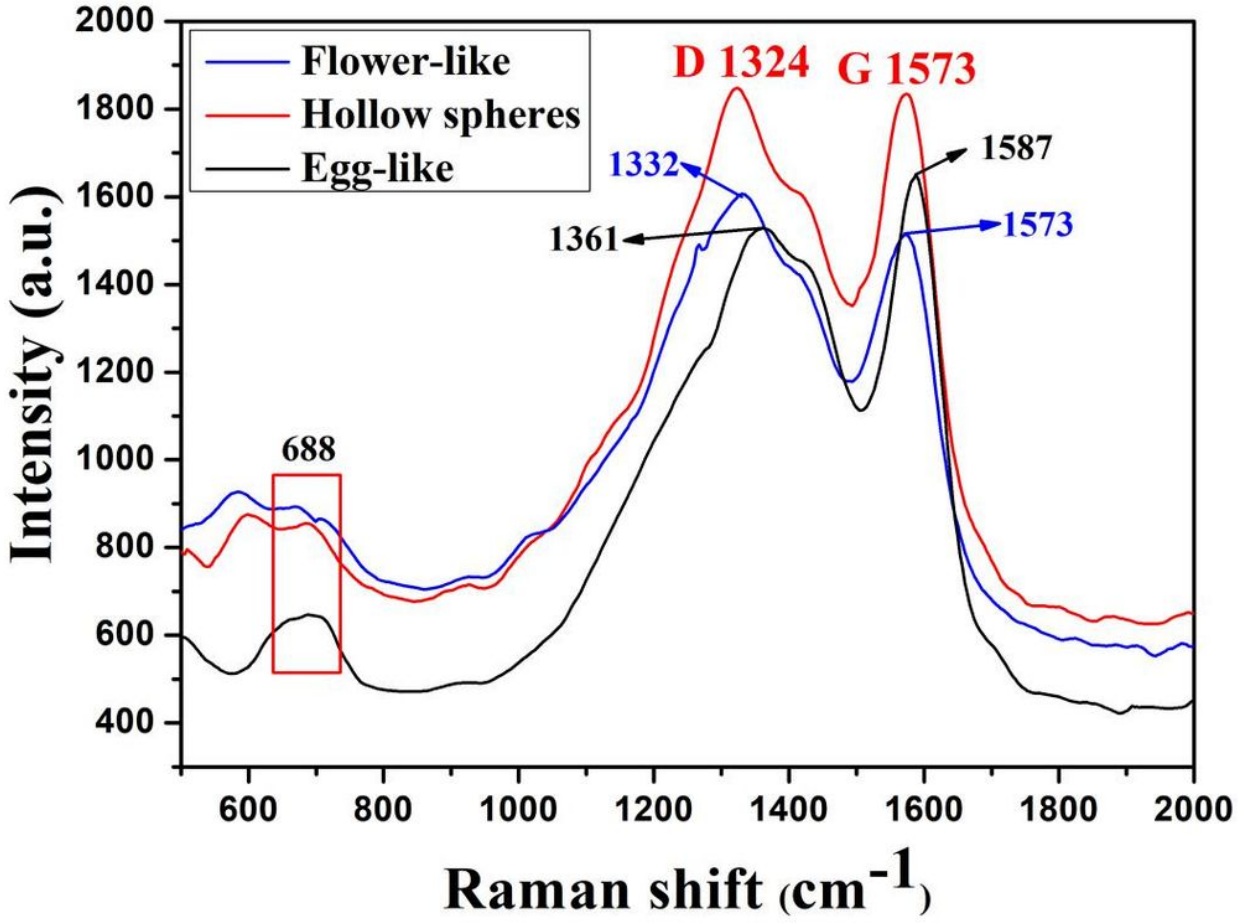

Figure 7

Raman spectra of Fe3O4@C flower-like, hollow spheres, and egg-like microstructures.

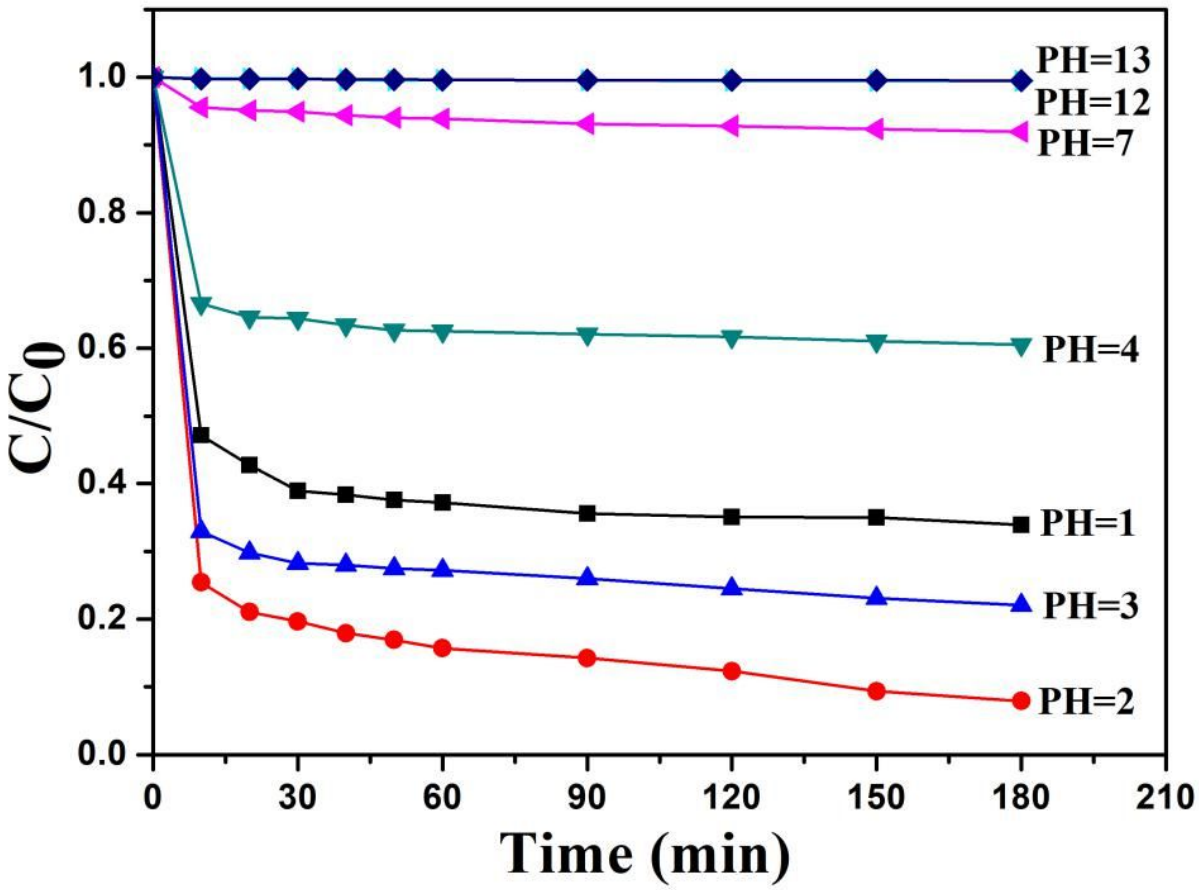

Figure 8

Relationship between the adsorption rate and time for the adsorption of Cr(VI) by the as-prepared Fe3O4@C hollow spheres, obtained at different PH value.

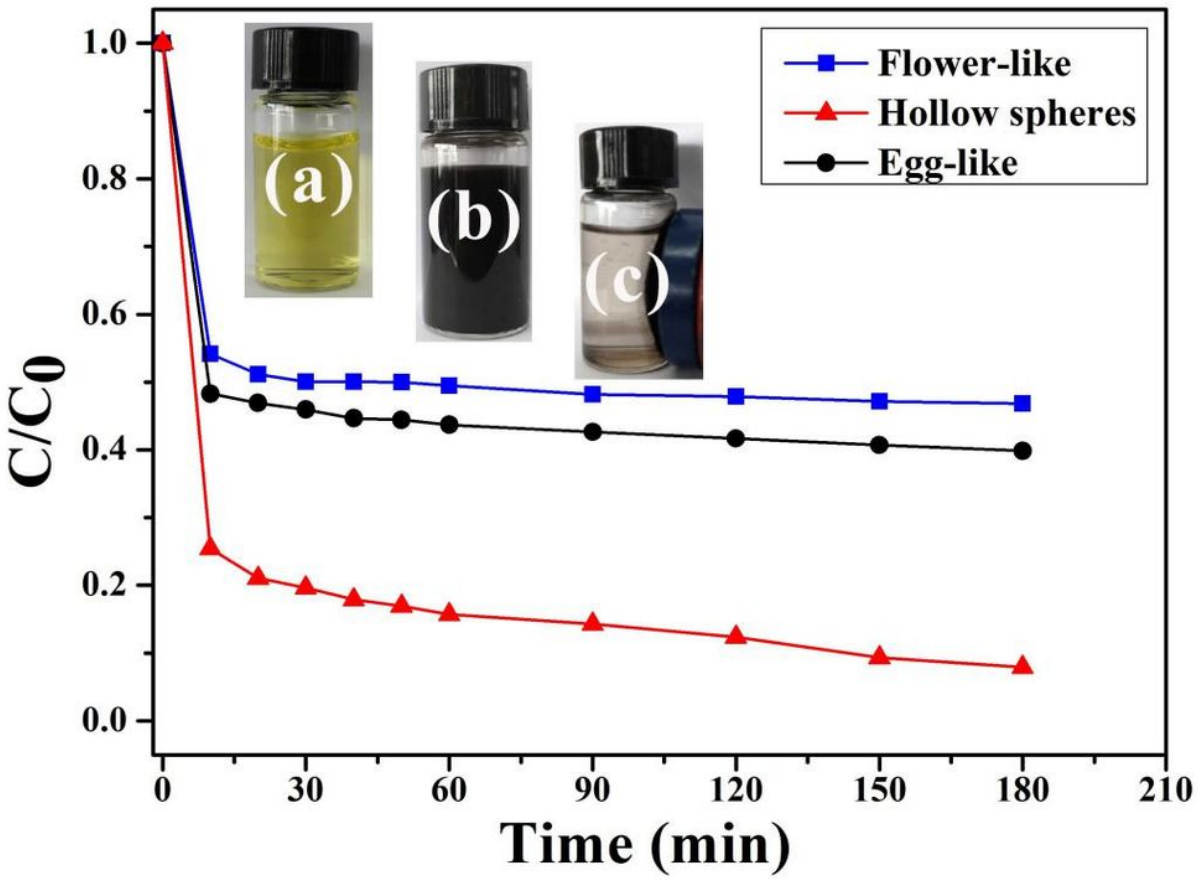

Figure 9

Relationship between the adsorption rate and time for the adsorption of Cr(VI) by the as-prepared Fe3O4@C flower-like, hollow spheres, and egg-like microstructures. C0(in mg L-1) is the initial concentration of the Cr(VI) solution and C(in mg L-1) is the concentration of Cr(VI) in the solution at different intervals during the adsorption process.

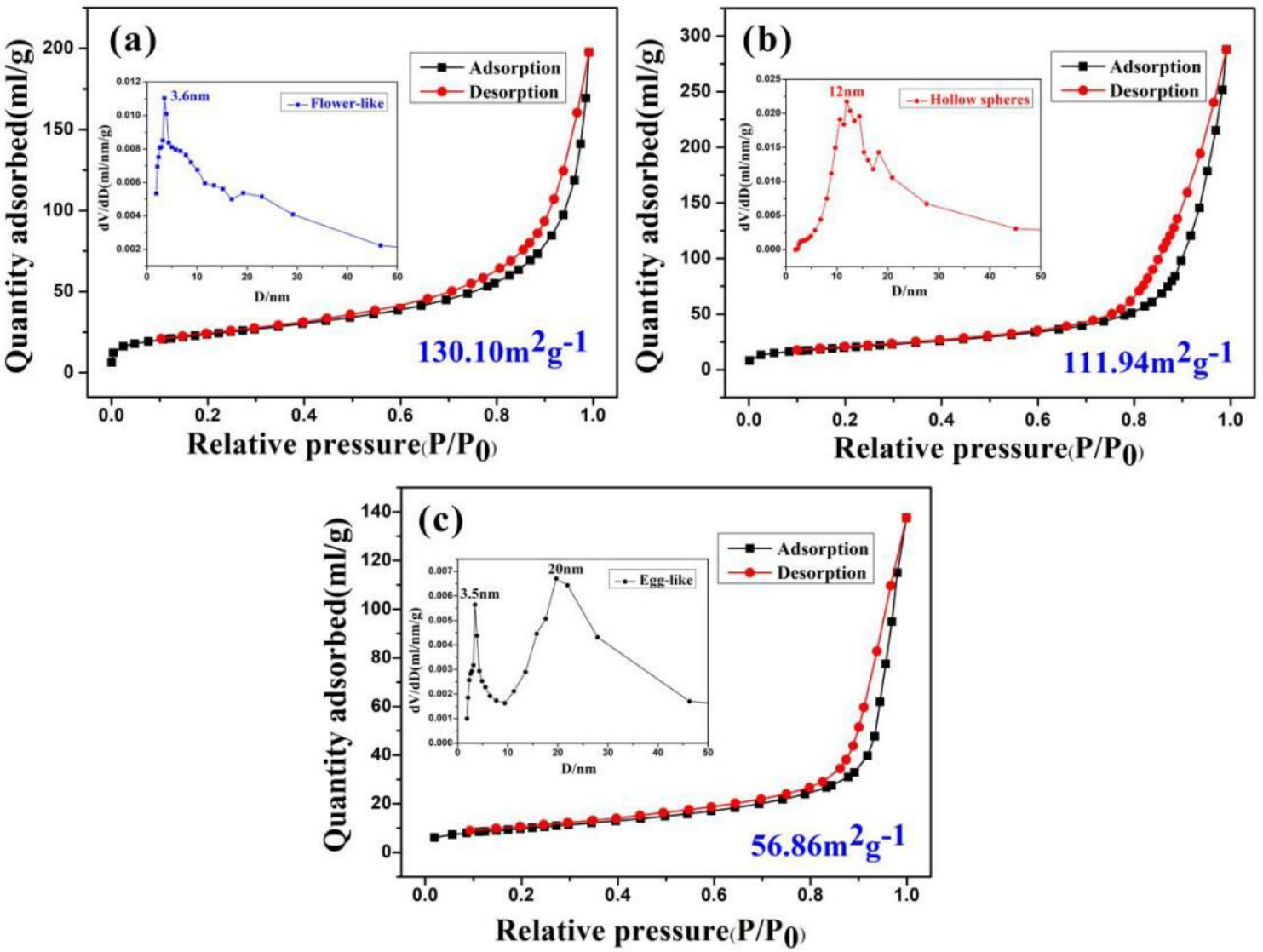

Figure 10

N2 adsorption-desorption isotherm and pore size distribution of Fe3O4@C flower-like, hollow spheres, and egg-like microstructures.

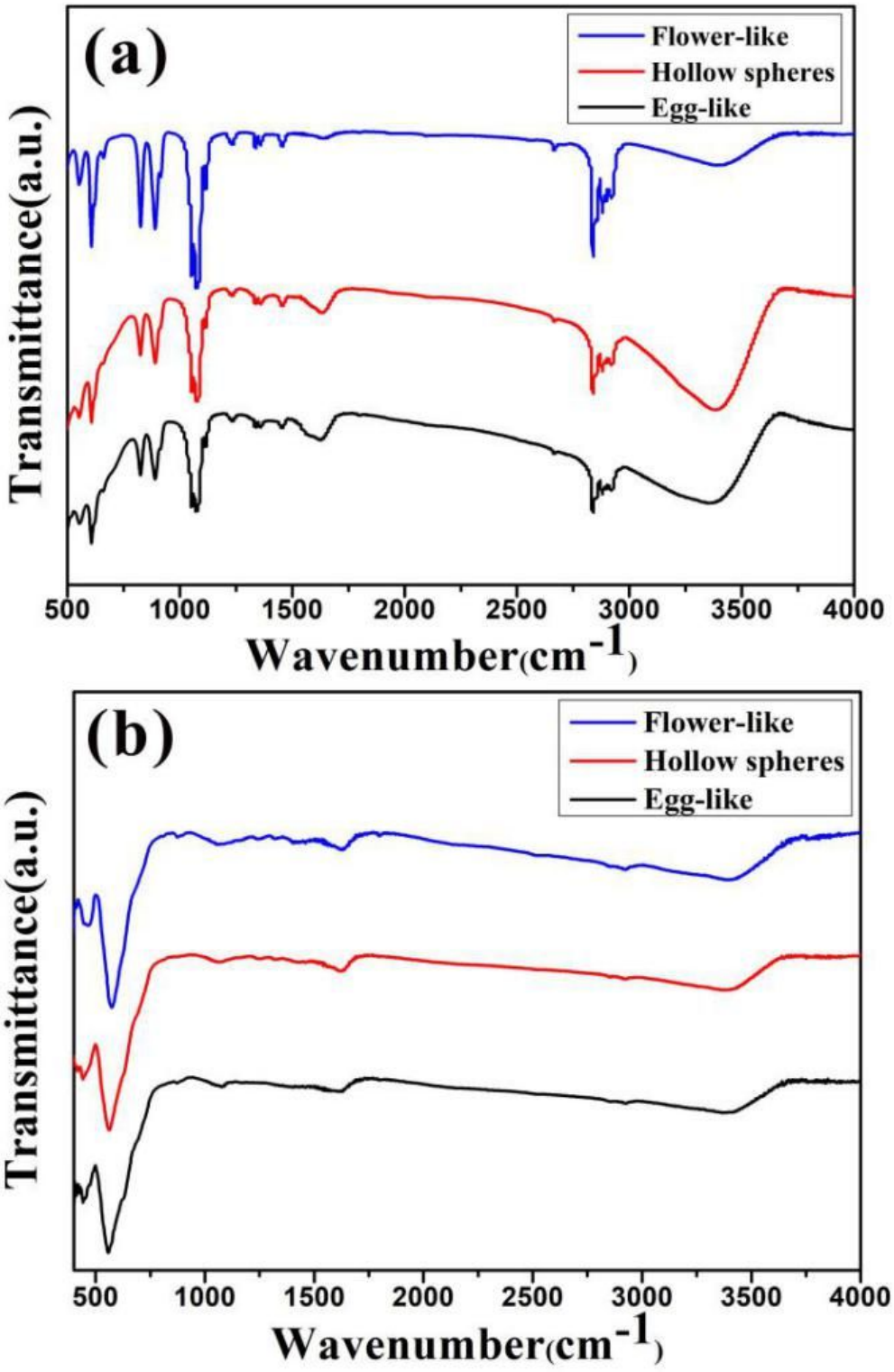

Figure 11

FTIR spectra of Fe3O4@C flower-like, hollow spheres, and egg-like microstructures (a) before annealing and (b) after annealing.